Functional Reorganization of the Visual Dorsal Stream as Probed by 3-D Visual Coherence in Williams Syndrome

Inês Bernardino[1], José Rebola[1], Reza Farivar[2,3], Eduardo Silva[4], and Miguel Castelo-Branco[1]

Abstract

■ Object and depth perception from motion cues involves the recruitment of visual dorsal stream brain areas. In 3-D structure-from-motion (SFM) perception, motion and depth information are first extracted in this visual stream to allow object categorization, which is in turn mediated by the ventral visual stream. Such interplay justifies the use of SFM paradigms to understand dorsal–ventral integration of visual information. The nature of such processing is particularly interesting to be investigated in a neurological model of cognitive dissociation between dorsal (impaired) and ventral stream (relatively preserved) processing, Williams syndrome (WS). In the current fMRI study, we assessed dorsal versus ventral stream processing by using a performance-matched 3-D SFM object categorization task. We found evidence for substantial reorganization of the dorsal stream in WS as assessed by whole-brain ANOVA random effects analysis, with subtle differences in ventral activation. Dorsal reorganization was expressed by larger medial recruitment in WS (cuneus, precuneus, and retrosplenial cortex) in contrast with controls, which showed the expected dorsolateral pattern (caudal intraparietal sulcus and lateral occipital cortex). In summary, we found a substantial reorganization of dorsal stream regions in WS in response to simple visual categories and 3-D SFM perception, with less affected ventral stream. Our results corroborate the existence of a medial dorsal pathway that provides the substrate for information rerouting and reorganization in the presence of lateral dorsal stream vulnerability. This interpretation is consistent with recent findings suggesting parallel routing of information in medial and lateral parts of dorsal stream. ■

INTRODUCTION

The extraction of 3-D information is performed by our visual system through the use of various visual cues including motion signals (Wallach & O'Connell, 1953). The study of 3-D visual coherence from motion cues can be studied using 3-D structure-from-motion (SFM) paradigms (Wallach & O'Connell, 1953). These paradigms included stimuli composed of a large set of coherent dots enabling the formation of 3-D shape percepts (typically an object or face shape). Importantly, shape extraction can only be achieved when the dots are moving because otherwise it remains invisible. It is therefore essential to integrate motion cues over time to be able to extract 3-D shape information. As a result, this experimental task allows to understand how motion and shape information are integrated and to investigate the complementary nature of their processing modules (Ungerleider & Mishkin, 1982).

Motion information processing has been reported to be computed in several brain areas along the dorsal visual stream, such as V3A, MT^{+}/V5 (Tootell et al., 1995, 1997), V6 (Pitzalis, Fattori, & Galletti, 2013; Pitzalis et al., 2010; Galletti, Fattori, Gamberini, & Kutz, 1999) intraparietal sulcus (IPS), namely, putative areas VIP and 2v, as well as the precuneus (Cardin & Smith, 2009; Grefkes & Fink, 2005). More recently, a new area, the cingulated sulcus visual area, was found to be implicated in egomotion processing (Cardin & Smith, 2009; Wall & Smith, 2008). Regarding perceptual categorization, several areas in the ventral stream have been described to be tuned to the preferential processing of specific object classes (LOC, FFA, PPA; Grill-Spector, Kourtzi, & Kanwisher, 2001; Epstein, Harris, Stanley, & Kanwisher, 1999; Kanwisher, McDermott, & Chun, 1997) although the category specificity has been also demonstrated to be relative (Haxby et al., 2001). Moreover, areas along the dorsal visual stream have been also shown to be recruited during object categorization, namely, the ventral caudal IPS (cIPS) and an occipital region just ventrolateral to it (Schendan & Stern, 2007).

Concerning 3-D SFM stimuli, which require integration of shape and motion, an extended network of cortical regions spanning the occipital, posterior parietal, and also posterior temporal cortices has been identified (Graewe, Lemos, et al., 2012; Klaver et al., 2008; Peuskens et al., 2004; James, Humphrey, Gati, Menon, & Goodale, 2002;

[1]University of Coimbra, [2]Harvard Medical School and Massachusetts General Hospital, [3]McGill University, [4]University Hospital Coimbra

Journal of Cognitive Neuroscience 26:11, pp. 2624–2636
doi:10.1162/jocn_a_00662

Paradis et al., 2000; Orban, Sunaert, Todd, Van Hecke, & Marchal, 1999). In particular, areas along the IPS and the lateral occipital complex (LOC) have been typically identified across studies as showing increased activation in response to this type of objects (Klaver et al., 2008; James et al., 2002; Orban et al., 1999). Less consistent findings have been reported in areas V1, V3A, and V5/MT possibly because of distinct task requirements and the fact that these regions underlie lower-level motion processing (Murray, Olshausen, & Woods, 2003; Paradis et al., 2000).

Because SFM stimulus perception involves the detection of coherent motion cues to extract 3-D shape information, an ideal model to study integration across dorsal and ventral visual streams would be a cognitive dissociation model with altered 3-D SFM perception. Such a neurological model characterized by dorsal–ventral visual stream dissociation actually exists. This is the case of Williams syndrome (WS), which is a rare genetic neurodevelopmental disorder characterized by dorsal stream dysfunction in the presence of a relatively preserved ventral stream function (Meyer-Lindenberg et al., 2004; Paul, Stiles, Passarotti, Bavar, & Bellugi, 2002; Atkinson et al., 1997). The dorsal stream vulnerability in this condition has been explored in relation to predominant visuospatial impairments, including motion detection deficits (Reiss, Hoffman, & Landau, 2005). These impairments have been demonstrated in tasks requiring 2-D and 3-D motion coherence processing (Atkinson et al., 2003, 2006). Importantly, object and depth perception from motion cues was also reported as being affected in this condition (Castelo-Branco et al., 2007; Mendes et al., 2005) with WS participants exhibiting impairments in 3-D SFM perception into a larger extent than those found in 2-D motion tasks (Mendes et al., 2005). The electrophysiological neural underpinnings of such impairments in 3-D coherent perception were investigated in a previous EEG study (Bernardino, Castelhano, Farivar, Silva, & Castelo-Branco, 2013), where we identified atypical neural responses to 3-D SFM conditions as revealed by distinct ERP waveform components. To investigate the cortical generators of these distinct neural responses, source localization analyses demonstrated more posterior (occipital) SFM-related sources in the WS group as compared with controls, who showed more parietal sources. These findings suggested reorganization of responses to 3-D SFM stimuli in WS but could not finely dissect the neural correlates of such reorganization.

In the current study, we conducted an fMRI study employing a 3-D SFM visual integrative task in which local motion cues drive 3-D shape perception. We aimed at investigating the nature of the dorsal–ventral visual stream function during altered 3-D coherent perception in WS. Given the proposed dorsal (impaired) versus ventral (relatively preserved) dissociation in WS (Atkinson et al., 2003; Paul et al., 2002), we expected to observe neural reorganization of responses to 3-D SFM stimulus in WS, in particular in the dorsal stream. We also tested the impact of such putatively changed responses in ventral visual stream regions that are connected to the dorsal stream. To better assess the nature and specificity of the neural substrates of 3-D SFM perception in WS, we conducted an SFM feature experimental task in which we manipulated the depth information (two different depth levels) because depth cues are known to influence 3-D SFM perception. We were interested in mapping the regions that responded to 3-D SFM stimuli in both groups and then investigate the response of those regions (SFM feature ROIs) to simple motion stimuli (2-D coherent moving dots and static dots) as well as other types of high-level visual stimuli (static faces, places, objects, and scrambled images). This approach allows us to examine if the altered pattern of brain responses to 3-D SFM stimuli expected in WS is confined to this complex type of stimuli or, on the other hand, is already present concerning the perception of other visual stimuli.

METHODS

Participants

A total of 20 participants took part in the study, namely, 10 WS patients and 10 healthy control participants. Because of exclusion criteria concerning excessive movement during the fMRI acquisition (see details below) or inability to remain inside the scanner until the end of the acquisition, four participants (three WS and one control) were excluded from the analysis. As a result, seven WS patients aged between 15 and 37 years (mean ± *SE* = 21.57 ± 3.01) and nine chronological age-matched control participants aged between 15 and 29 years (mean ± *SE* = 21.22 ± 1.61) were included for the final analysis.

The WS participants were identified from a large sample of participants who had previously participated in our studies (Bernardino et al., 2012, 2013). The selection was based on the age (≥15 years) and on the ability to cooperate in the fMRI acquisition. The diagnosis was confirmed by genetic examinations including the FISH analysis, which confirmed the typical hemizygous 7q11.23 deletion (~1.55 Mb) in all patients, demonstrating a relatively homogeneous genetic basis for our clinical group. None of the WS participants was diagnosed with attention dysfunction hyperactivity disorder or was taking medication to control for attention and behavioral problems or depression symptoms. The Social Communication Questionnaire, which is a screening test for ASD symptoms, was completed by the participants' parents to exclude comorbidity with ASD (Rutter, Bailey, & Lord, 2003). The positive cutoff for ASD is 15, and all participants scored below. All WS patients underwent a complete ophthalmological examination performed by an experienced ophthalmologist, including best-corrected visual acuity (Snellen optotypes), complete oculomotor examination, stereopsis evaluation using the Randot test, slit lamp examination of anterior chamber structures, and fundus examination. No abnormalities that could affect vision were

identified. When necessary, the correction to normal vision was ensured using specific eyeglasses compatible with the magnetic field. Given that WS patients exhibited high levels of anxiety and hypersensitivity to the sound (Blomberg, Rosander, & Andersson, 2006), a research staff member worked with each patient so they were previously familiarized with the MRI sounds and were able to attend and perform experimental tasks inside the scanner. A research assistant remained close to patients holding their hand to ensure that participants felt safe and stayed calm during the fMRI acquisition.

The control group included nine typically developing participants who were matched for chronological age (Mann–Whitney U test, $p > .05$), sex, and handedness with the WS group. Two WS patients and one control participant demonstrated left-hand dominance, as it was measured using the Edinburgh Inventory (Oldfield, 1971). The exclusion criteria for all participants included the presence of psychiatric or neurological pathologies, abnormal ophthalmological conditions, and the use of medication for treating depression.

All participants included in the study received the Portuguese adapted version of the Wechsler Intelligence Scale for Children, 3rd edition (Wechsler, 2003) or the Wechsler Adult Intelligence Scale, 3rd edition (Wechsler, 2008), according to the participant's age. The range of the intelligence quotient (IQ) in our clinical group confirmed the presence of moderate mental retardation. The demographic characterization of both groups is summarized in Table 1.

This study was conducted in accordance to the Declaration of Helsinki and was approved by the local ethics committees of the Faculty of Medicine of the University of Coimbra. Parents of participants, or, when appropriate, the participants themselves provided verbal and written informed consent.

Materials and Procedure

In this study, an experimental task using 3-D SFM stimuli was conducted as well as separate runs presenting simple motion stimuli and high-level visual categorical stimuli. The SFM and the high-level visual object runs were presented using Presentation 15.0 software (Neurobehavioral Systems, Berkeley, CA), and the simple motion run was presented using Matlab (R2009b). Stimuli were projected with an LCD projector (SilentVision 6011, Avotec, Inc., Stuart, FL) onto a rear-projection Fujitsu Siemens type screen (1024 × 768, refresh rate 60 Hz). The screen was viewed at a distance of 45.5 cm with an angled mirror positioned on the head coil and subtended 30.3° width and 23.1° height of visual angle.

During the fMRI acquisition, the participants' eye movements were monitored using a video recording system to ensure compliance and safety and to verify that wakefulness was maintained (RealEye 5721, Avotec, Inc.).

SFM Feature Localizer Task: Stimuli and Design

An experimental task using videos of SFM-defined faces and chairs with the duration of 980 msec (for further details, see Bernardino et al., 2013; Graewe, De Weerd, Farivar, & Castelo-Branco, 2012; Farivar, Blanke, & Chaudhuri, 2009) was conducted to localize the regions that responded to SFM stimulus in both groups Figure 1A. Face stimuli consisted of 3-D laser-scanned heads from the Max-Planck Face Database, and chair stimuli were selected from a chair model database. Both face and chair stimuli were rendered using a unique texture mapping technique (Troje & Bulthoff, 1996) and rotated in a cycle from −22.5° to 22.5° centered at the frontal plane. Stimulus depth information was parametrically manipulated at two different levels resulting in an overall 2 (stimulus category) × 2 (depth levels) design. The depth levels were parameterized in terms of anterior–posterior range in which "full" and "flat" depth conditions had 10% and 90% less depth, respectively, using the posterior plane as a reference (see Figure 1B).

The experimental task consisted of three separate runs with the duration of approximately 4 min each. A slow event-related design was employed in which four experimental conditions (Full Face, Full Chair, Flat Face, and Flat Chair) were randomly presented. A total of

Table 1. Demographic Characteristics

	WS (n = 7)		*Control (n = 9)*	
	Mean (SE)	*Range*	*Mean (SE)*	*Range*
Chronological age (years)	21.57 (3.01)	15–37	21.22 (1.61)	15–29
FSIQ (WISC-III or WAIS-III)	54.29 (4.57)	42–75	120.79 (3.26)	106–136
Handedness (left:right)	2:5		1:8	
Sex (M:F)	3:4		5:4	

WS = WS group; Control = control group; FSIQ = full-scale intellectual quotient; WISC-III = Wechsler Intelligence Scale for Children, 3rd ed.; WAIS-III = Wechsler Adult Intelligence Scale, 3rd ed.

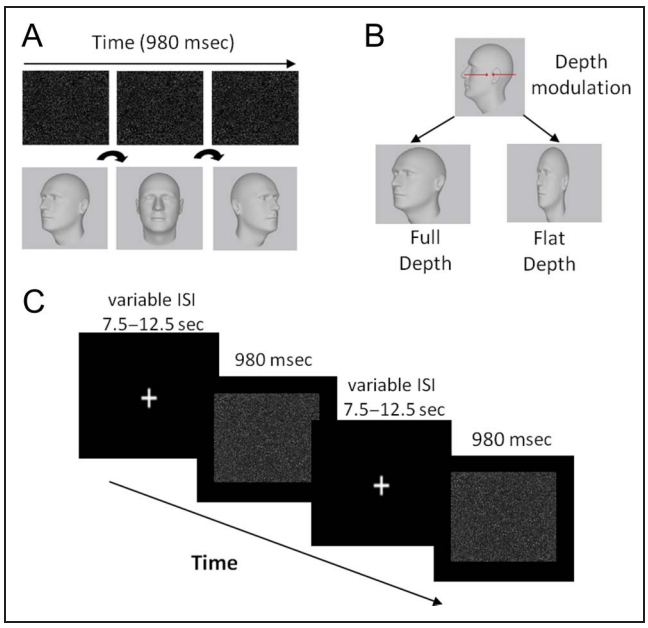

Figure 1. SFM feature localizer task: stimuli and paradigm (adapted from the studies of Graewe, De Weerd, et al., 2012; Graewe, Lemos, et al., 2012). (A) SFM faces and chairs rotated from left to right in one cycle and were shown during 980 msec. Object perception is rendered possible by integration of the moving dot pattern, the object being physically absent when the rotation/motion is absent. (B) The depth modulation resulted in SFM stimulus conditions with two different depth levels (full and flat depth) parameterized in terms of anterior–posterior range. (C) Face and chair stimuli were presented randomly at one of the two depth levels separated by a variable 7.5–12.5 sec ISI in which participants were asked to fixate a cross in the center of the screen. Note that the images of the heads included in the figure just illustrate the structure in the SFM stimuli and do not represent (because they are physically absent and not visible in static images) the exact percept during the movies' presentation.

12 trials per condition were obtained. The participants viewed a fixation cross followed by the SFM animation and were required to press a button whenever the presented stimulus was a face (see Figure 1C). Responses were provided using a button box (right hand index finger) after stimulus disappearance, during the variable interstimuli fixation interval (7.5, 10, 12.5 sec).

Simple Motion Task: Stimuli and Design

In the motion run, participants passively viewed coherently moving texture patterns alternated with the same static pattern. Both moving and static patterns (12.6° × 12.6°) were composed of arrays of 600 dots with 0.3° diameter. The dots were white and were shown in a dark background. In the moving patterns, dots could be moving in four directions (left, right, up, down) at a constant speed of 5°/sec. The run lasted 4.18 min and consisted of 30-sec blocks for each type of stimulus. In each block, six stimuli with 4.5-sec duration were included, separated by 500 msec of ISI. The blocks were separated by 10-sec periods of fixation.

High-level Visual Categorical Task: Stimuli and Design

During the high-level visual categorical run, participants viewed static grayscale photographic images of faces, places (landscapes, skylines), objects (tools, cars, chairs), and scrambled versions of objects (9.5° × 9.5°). Stimuli were presented on a dark background centered at fixation (fixation cross with radius 0.15° in middle of display). Each stimulus category (faces, places, objects, scrambled images) was presented during three pseudorandomly ordered blocks performing a total of 12 blocks. Each block lasted 20 sec separated by 10-sec fixation baseline interval. Images (20 per block) were presented during 800 msec with 200 msec of ISIs. Participants were instructed to fixate on each image and were asked to press a button whenever an image was identical to the previous one ("1-back task"). Three repetitions per block were employed. This task was administered to ensure stable attention levels.

Imaging Data Acquisition and Preprocessing

Scanning was performed in a 3T Siemens Trio scanner at the Portuguese Brain Imaging Network using a 12-channel head coil. For structural whole-brain images, two high-resolution T1-weighted MP-RAGE sequences (1 × 1 × 1 mm voxel size, 160 slices, repetition time [TR] = 2.3 sec, echo time [TE] = 2.98 msec, flip angle (FA) = 9°, and field of view [FOV] = 256 × 256) were conducted. Standard T2*-weighted gradient EPI was used for functional task runs (EPI, interleaved slice acquisition order, voxel size = 2 × 2 × 4 mm, 29 slices, TR = 2.5 sec, TE = 49 msec, in-plane matrix = 128 × 128, FA = 90°, FOV = 256 mm) covering the entire brain. Functional images for face and motion localizers were acquired using a gradient-echo T2* -weighted echo planar (2.5 × 2.5 × 3.5 voxel size, 25 slices, TR = 2 sec, TE = 47 msec, in-plane matrix = 102 × 102, FA = 90°, FOV = 256 mm).

The data were preprocessed and analyzed using Brainvoyager QX 2.4. We applied slice scan time correction, temporal high-pass filtering (two cycles per run), and correction for small within-run head movements. Participants exceeding 3 mm were excluded from further analysis (n = 2 WS, one control). Before group analysis, the images were spatially smoothed using 4 mm (for experimental SFM runs) and 5 mm (for face/object and motion runs) FWHM Gaussian kernel and then were transformed into Talairach coordinates, which have been extensively used in studies in WS (O'Hearn et al., 2011; Boddaert et al., 2006; Eckert et al., 2006; Meyer-Lindenberg et al., 2004).

Data Analysis

All the statistical analyses were performed using IBM SPSS Statistics 19 (IBM, NY, www.ibm.com/software/analytics/

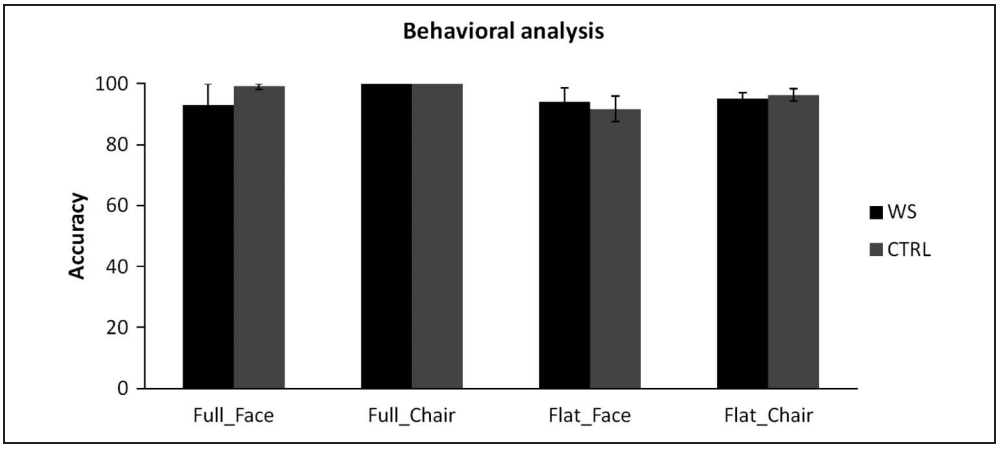

Figure 2. Performance across SFM category and depth conditions in WS and typical developing controls. Groups are performance-matched under the conditions of our experiment (Mann–Whitney test, $p > .05$). Note the absence of standard error bars in the "Full Chair" condition indicating that the performance for both groups is at ceiling level, confirming this condition as a control to assure that participants understood the instructions. Error bars show *SEM*. WS = WS group; CTRL = chronological age-matched typical developing control group.

spss/) and the BrainVoyager QX 2.4 software (Brain Innovation, Maastricht, the Netherlands).

Behavioral Data

Nonparametric statistics (Mann–Whitney *U* tests) were carried out for all statistical analyses to avoid biases because of deviations from normality and variance heterogeneity.

Functional Data

To localize the SFM feature ROIs, a three-way random-effects (RFX) ANOVA with within-factor Depth (full vs. flat) and Category (face and chairs) and between-factor Group (control vs. WS) was conducted. Then, whole-brain statistical maps for group effect were computed. This map revealed areas for which there are fundamental differences between groups irrespective of other factors. The areas related to visual processing were defined as SFM feature ROIs. Additionally, we computed an interaction Depth × Group map to assess regions for which, across groups, flat and full conditions are differentially affected. Resulting F maps were thresholded at $p < .05$ corrected for multiple comparisons through cluster-level statistical threshold estimation based on Monte Carlo simulation with 1000 iterations. Further analysis of the identified regions was performed with a ROI-based random effects general linear model (GLM) to identify the task conditions that drove the significant RFX ANOVA interaction and group effects.

With the purpose of examining the functional properties of the identified SFM feature ROIs, for each region, a ROI-based ANOVA was performed to assess its response to both motion and high-level visual runs. Post hoc *t* tests were also computed whenever significant group or interaction effects were found. These latter ANOVAs were conducted to assess if the areas of differential processing between groups identified with the SFM stimuli were restricted to that paradigm

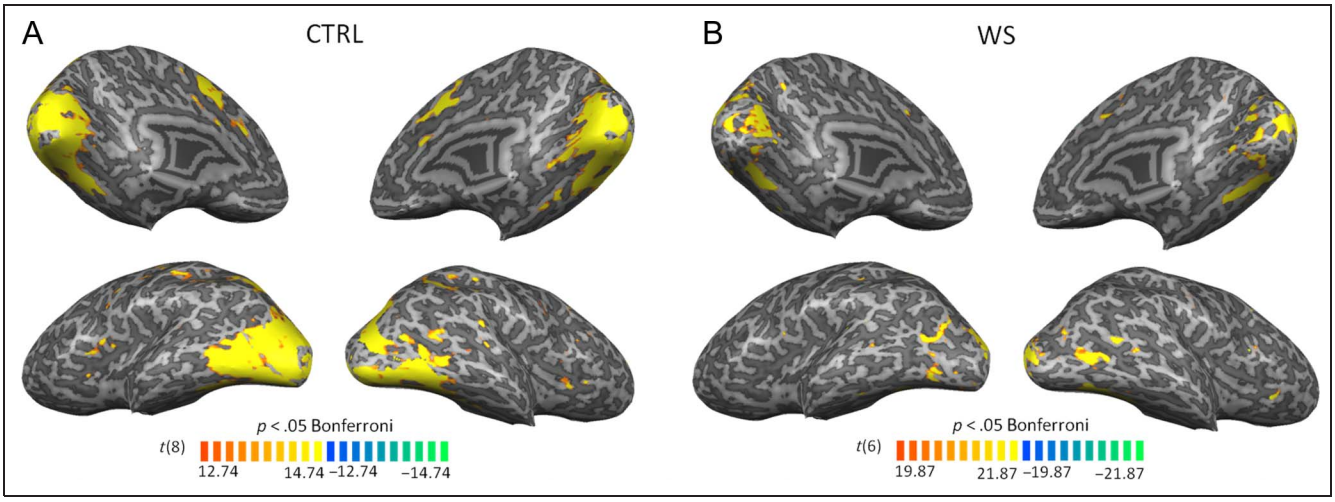

Figure 3. SFM localizer task: brain activation patterns. The overall activation of the control group (A) and the WS group (B) in response to the SFM task (full and flat depth levels together). Light gray represents gyri, and dark gray represents sulci of 3-D reconstructed views of the left and right hemispheres. WS = WS group; CTRL = chronological age-matched typical developing control group.

or already exhibited differences for lower-level stimuli such as static images or unstructured motion.

Finally, for an appreciation of whole-brain response similarities and differences across groups, separate statistical activation maps were computed and superimposed in 3-D renderings for each experimental task: SFM feature localizer task, simple motion task, and high-level visual categorical task. The differences between the groups were also computed for the simple motion and high-level visual categorical tasks (Figures 3–5).

Additionally, correlation analyses were performed between fMRI SFM-defined objects responses and IQ to understand if the intelligence levels were correlated with the pattern of activation found in WS. A whole-brain RFX ANOVA with the covariate IQ was computed. The resulting statistical maps did not show any region in which the β weights and the IQ scores correlated significantly.

RESULTS

Behavior

Behavioral analysis revealed that WS and control groups achieved similar categorization performance in the SFM task for all categorical stimuli and depth conditions ($p > .05$, Mann–Whitney U). The same pattern was found regarding RT measures, with no significant differences between the groups ($p > .05$, Mann–Whitney). In summary, both groups are performance-matched under the conditions of our experiment (Figure 2).

Patterns of Brain Activation in Response to the Experimental Tasks

To better appreciate patterns of responses across groups, the pattern of activation in response to SFM (Figure 3),

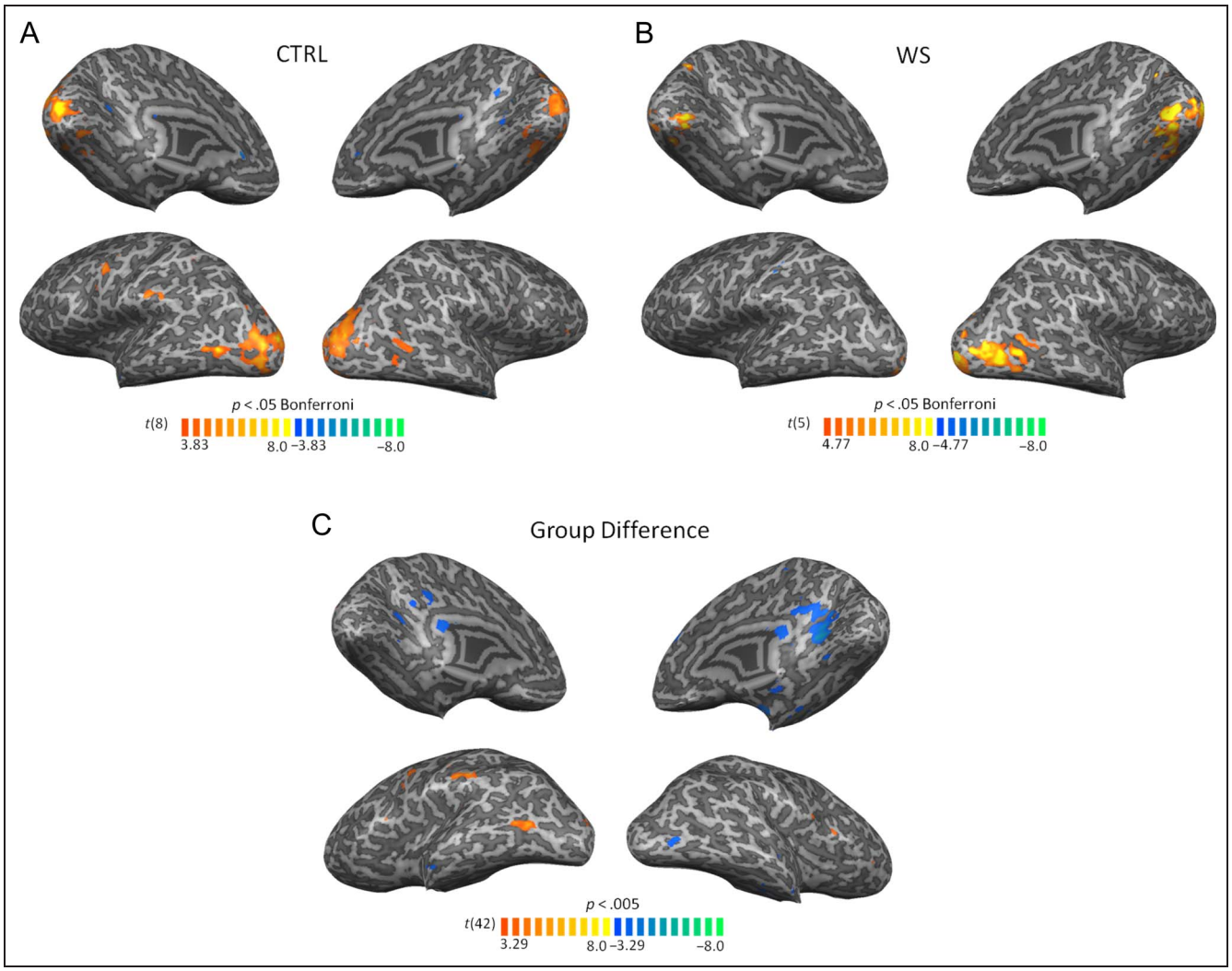

Figure 4. Simple motion experimental task: brain activation patterns. The top illustrates the pattern of activation of the control group (A) and the WS group (B) for the contrast motion > no motion. (C) The bottom illustrates the significant differences in brain activations between patients with WS and controls, regarding the simple motion experimental task. Cold color clusters depict regions where activation was higher for individuals with WS than controls. Warm color clusters depict regions where activation was lower for individuals with WS than controls. Note a more medial pattern of activation in the WS group in response to motion stimuli. Light gray represents gyri, and dark gray represents sulci of 3-D reconstructed views of the left and right hemispheres. WS = WS group; CTRL = chronological age-matched typical developing control group.

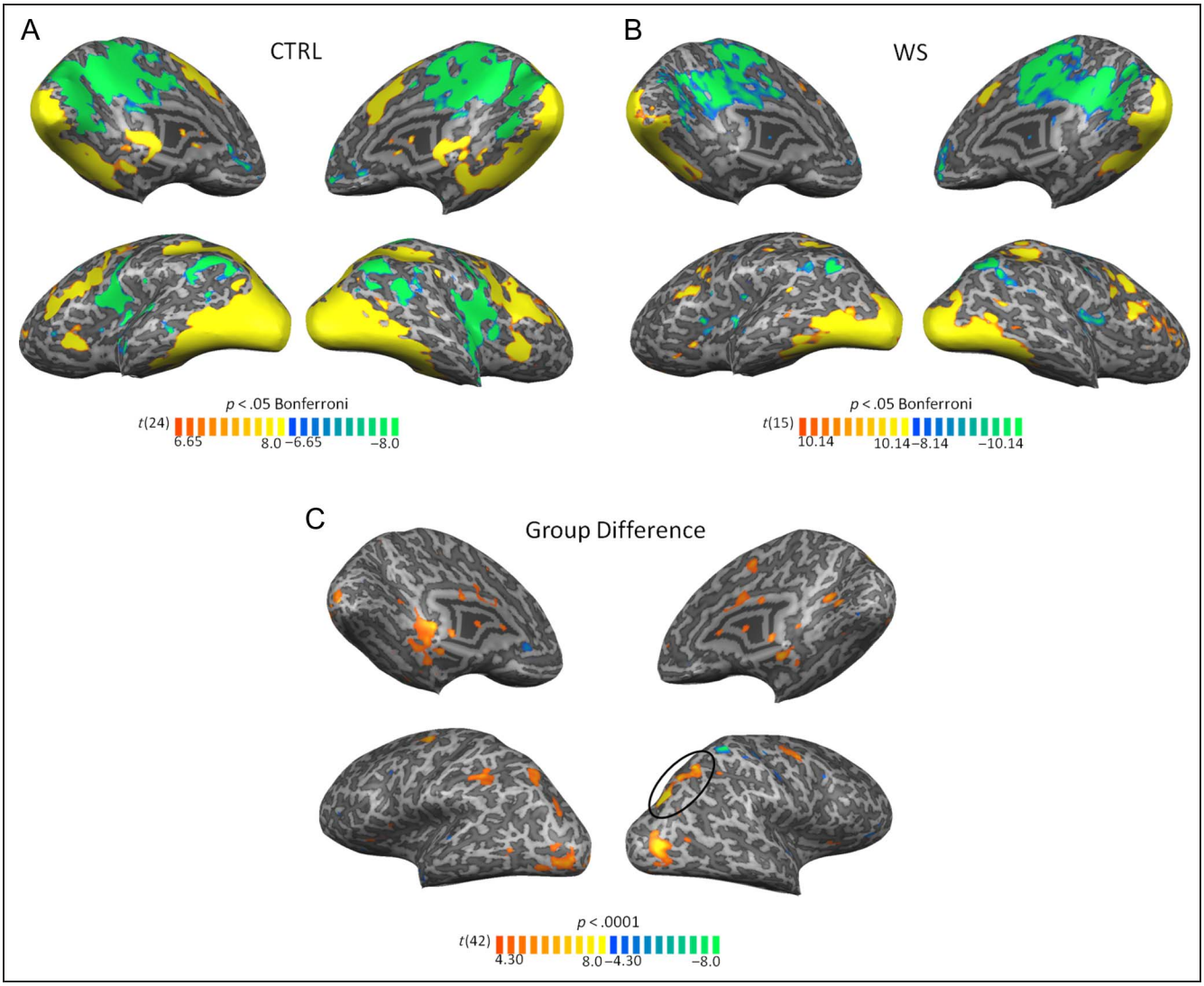

Figure 5. High-level visual categorical experimental task: brain activation patterns. The top illustrates the pattern of activation of the control group (A) and the WS group (B) in response to the static images of different categories (faces, places, objects, and scrambled images together). (C) The bottom illustrates the significant differences in brain activations between patients with WS and controls, regarding the high-level categorical stimuli. Cold color clusters depict regions where activation was higher for individuals with WS than controls. Warm color clusters depict regions where activation was lower for individuals with WS than controls. Note subtle differences between the groups in the degree of activation in areas of both dorsal (signalled by a circle) and ventral visual pathways in response to a broad range of high-level stimulus categories. Light gray represents gyri, and dark gray represents sulci of 3-D reconstructed views of the left and right hemispheres. WS = WS group; CTRL = chronological age-matched typical developing control group.

simple motion (Figure 4), and high-level categorical (Figure 5) stimuli is shown for each group separately. Additionally, the group differences in response to both simple motion (Figure 4C) and high-level categorical experimental tasks were computed (Figure 5C). The group differences for the 3-D SFM feature localizer task were also performed and shown in Figure 6 (for better illustration of the defined SFM feature ROIs).

The pattern of brain activation for the simple motion task reveals that patients with WS recruit more medial areas than the control group, which recruited the expected hMT^+ region. Concerning the global activation maps for the high-level categorical task, we observed subtle differences between the groups in the degree of activation of areas belonging to both ventral and dorsal visual pathways. WS patients exhibit overall lower activation than the controls in the referred areas. Interestingly, for more complex categorical stimuli (static images of high-level visual categories), we cannot identify regions that are more active in the WS group than in controls, contrary to what occurred for the simple motion task.

fMRI: Whole-brain Analysis of Between-group Effects in SFM Task

The whole-brain RFX ANOVA revealed significant Group effects in bilateral cIPS and LOC (larger activation for control participants, see below) as well as in cuneus,

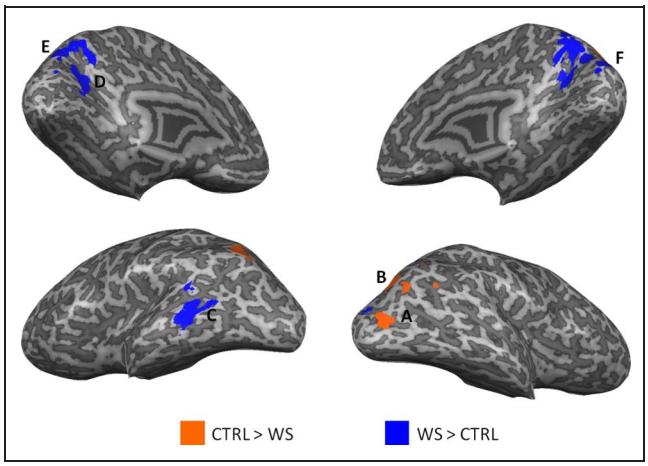

Figure 6. Representation of SFM feature ROIs revealed by RFX ANOVA group effects. Blue clusters depict visual regions where activation was higher for individuals with WS than controls ($p < .05$, cluster corrected for multiple comparisons). Orange clusters depict visual regions where activation was lower for individuals with WS than controls. Note the more dorsolateral activation pattern in controls recruiting areas in the (A) LOC (near the area hMT$^+$) and (B) cIPS. In contrast, there is a shift to the midline observed for SFM responses in WS, activating areas such as (D) retrosplenial cortex, (E) precuneus, and (F) cuneus (regions corresponding to PO/V6 areas). (C) refers to MTG. Light gray represents gyri, and dark gray represents sulci of 3-D reconstructed views of the left and right hemispheres. WS = WS group; CTRL = chronological age-matched typical developing control group.

precuneus, and retrosplenial cortex (larger activation for WS participants, see below; Figure 6). This contrast between the pattern observed in controls and the more medial activation seen in WS is summarized in Table 2 ($F \geq 12.84$; $p < .05$, corrected for multiple comparisons) and further highlighted in Figure 6. There was no significant Group × Depth interaction effect. ROI-based post hoc t tests confirmed higher and more medial activation for WS compared with controls in response to Flat depth (10%) stimuli in the right cuneus, right precuneus, left retrosplenial cortex, as well as left middle temporal gyrus (MTG). Interestingly, Full depth (90%) conditions showed increased activation in WS only for the MTG. The same analysis revealed enhanced neural responses for controls compared with WS in bilateral cIPS and right LOC (LO near the area hMT$^+$) for both Full and Flat depth levels (for further details on statistical significance, see Table 2). Somatosensory areas were also observed because of sensory stimulation (see Methods for details).

Interestingly, ventral stream category-specific areas traditionally defined by functional localizers did not show significant differences between controls and WS. This does not necessarily indicate that these areas presented a relatively spared function in WS. In fact, we may not identify group difference in these regions because they are characterized by high anatomical variability or because the small patches of activation did not survive to the rigorous correction for multiple comparisons applied. Additionally, the anatomical variability associated to the study of clinical populations and the reduced sample size of our study may contribute to the difficulty in observe less salient group effects. Interestingly, as we can observe in the Figure 5, the overall degree of activation of the WS participants in areas along the ventral visual stream is lower than in the control group in response to high-level visual categorical stimuli. This suggests that the activation

Table 2. Whole-brain RFX ANOVA Analysis: Summary of RFX-GLM Contrasts, Outputs, and Statistics

	Peak Talairach Coordinates					*Full Condition*		*Flat Condition*	
	x	*y*	*z*	*No. of Voxels*	*F*	*t*	*p*	*t*	*p*
WS > CTRL									
RH cuneus	14	−77	24	1323	14.24	−0.77	.458	−2.52	**.025**
RH precuneus	11	−62	42	2988	25.02	−1.20	.251	−2.67	**.019**
LH MTG	−56	−56	9	1542	21.97	−2.68	**.018**	−4.40	**.001**
RH retrosplenial cortex	23	−59	15	831	19.46	−1.03	.321	−1.06	.309
LH retrosplenial cortex	−22	−65	15	1038	12.84	−0.74	.474	−2.45	**.028**
CTRL > WS									
RH cIPS	23	−50	30	2121	20.64	5.08	**<.001**	4.15	**<.001**
LH cIPS	−31	−65	42	784	17.50	0.392	**.001**	2.724	**.016**
RH LO/near hMT$^+$	29	−74	9	350	13.54	3.871	**.002**	2.421	**.030**

Brain regions showing significant whole-brain RFX-ANOVA group effect ($p < .05$, corrected for multiple comparisons) and ROI-based GLM-RFX contrasts for group differences between responses to Full and Flat depth conditions. Negative t tests indicate higher β values for the WS group than for controls. Positive t tests indicate higher β values for the control group than for WS group. x, y, and z represent Talairach coordinates. Significant comparisons are marked in **bold**. WS = WS group; CTRL = chronological age-matched typical developing control group; RH = right hemisphere; LH = left hemisphere.

Table 3. ROI-based ANOVA: Static Images of High-level Visual Categories

	Group Effect		*Interaction Effect*		*Faces*		*Objects*		*Places*		*Scrambled*	
	F	*p*	*F*	*p*	*t*	*p*	*t*	*p*	*t*	*p*	*t*	*p*
WS > CTRL[a]												
RH cuneus	1.10	.314	0.84	.478	–	–	–	–	–	–	–	–
RH precuneus	0.84	.375	3.506	.024	0.11	.914	−1.91	.078	−2.25	**.04**	0.496	.628
LH MTG	3.93	.070	3.49	.025	−2.81	**.015**	−1.55	.145	−2.50	**.026**	−0.85	.412
RH retrosplenial cortex	0.458	.510	2.28	.094	–	–	–	–	–	–	–	–
LH retrosplenial cortex	1.59	.230	1.48	.236	–	–	–	–	–	–	–	–
CTRL > WS[a]												
RH cIPS	41.230	<.001	1.62	.200	5.97	**<.001**	6.03	**<.001**	7.95	**<.001**	5.00	**<.001**
LH cIPS	3.50	.084	1.86	.153	–	–	–	–	–	–	–	–
RH LO/near hMT$^+$	25.70	<.001	2.641	.063	3.29	**.005**	4.85	**<.001**	5.85	**<.001**	5.15	**<.001**

ROI-based ANOVA and GLM-RFX contrasts for group differences between responses to high-level visual categories in the regions revealed by SFM stimulation. Negative *t* tests indicate higher β values for the WS group than for controls. Positive *t* tests indicate higher β values for the control group than for WS group. Significant comparisons are marked in **bold**. WS = WS group; CTRL = chronological age-matched typical developing control group; RH = right hemisphere; LH = left hemisphere.

[a]Evidence from the SFM task analyses.

in areas belonging to the ventral visual pathway may also be atypical in the WS group although in a lower extent than the differences found in dorsal visual pathway areas.

The SFM feature ROIs previously identified (listed in Table 2 and shown in Figure 6) can be driven by different processing of motion extraction, shape processing, or other processes exclusive to 3-D SFM that require the integration of these features. In this manner, to assess their specificity, we analyzed the responses of these regions to our simple motion and high-level categorical

Table 4. ROI-based ANOVA: Simple Motion Coherence Stimuli

	Group Effect		*Interaction Effect*		*No Motion*		*Motion*	
	F	*p*	*F*	*p*	*t*	*p*	*t*	*p*
WS > CTRL[a]								
RH cuneus	9.39	.008	1.53	.236	−3.53	**.003**	−2.96	**.010**
RH precuneus	0.95	.347	0.88	.365	–	–	–	–
LH MTG	3.93	.069	3.49	.025	−3.14	**.007**	0.28	.235
RH retrosplenial cortex	6.22	.026	9.37	.009	−1.08	.299	−3.34	**.005**
LH retrosplenial cortex	5.39	.036	3.48	.083	−1.18	.133	−3.10	**.008**
CTRL > WS[a]								
RH cIPS	5.09	.041	0.96	.344	1.82	.090	2.58	**.022**
LH cIPS	0.00	.977	0.27	.609	–	–	–	–
RH LO/near hMT$^+$	9.43	.008	0.04	.940	2.76	**.015**	3.11	**.008**

ROI-based ANOVA and GLM-RFX contrasts for group differences between responses to simple motion coherence stimuli in the regions revealed by SFM stimulation. Negative *t* tests indicate higher β values for the WS group than for controls. Positive *t* tests indicate higher β values for the control group than for WS group. Significant comparisons are signaled with **bold**. RH = right hemisphere; LH = left hemisphere.

[a]Evidence from the SFM task analyses.

stimuli. We found that, in most cases, the altered response of these areas to 3-D SFM stimuli shows already significant between-group differences for either (or both) simple motion coherence or static images of high-level categories.

Regarding the responses to static images of high-level visual categories (faces, places, objects, scrambled images), we found significant group effects in the right cIPS and in the right LO and significant interaction effect in right precuneus, left MTG, and right LO (Tables 3 and 4 summarize the quantitative outcomes of statistical analyses). Post hoc *t* test analyses allowed us to investigate the differential response of these regions to these static stimuli categories (faces, objects, places, and scrambled images). We found increased activation in WS compared with controls in the right precuneus for place stimuli and in the left MTG for face and place stimuli. On the other hand, controls revealed, as expected, enhanced activity in right cIPS and in right LO for all high-level visual categories as compared with WS (see Table 3 for further details on statistical significance).

Concerning the simple motion coherence stimuli (2-D coherent moving dots vs. static dots), we found significant group effect in the right cuneus, bilateral retrosplenial cortex (increased in WS, see below), right cIPS and right LO (decreased in WS), and significant interaction effect in the left MTG and right retrosplenial cortex. Post hoc *t* tests allowed us to investigate the differential response of these regions to the alternating coherent dot motion and static dot stimuli. Accordingly, we found significantly increased activation in WS compared with controls in the cuneus and bilateral retrosplenial cortex in response to coherent 2-D motion stimuli and in the right cuneus and left MTG for static dot stimuli. On the other hand, controls revealed, as expected, significantly enhanced activity in right cIPS for motion stimuli and in the right LO for both stimuli as compared with WS (for further details on the statistical significance, see Table 4).

DISCUSSION

The current work is, to our knowledge, the first fMRI study identifying dorsal visual stream medial versus lateral reorganization underlying 3-D visual coherent perception in a cognitive dissociation model.

We used 3-D SFM stimuli to assess object and depth perception from motion cues and to investigate how dorsal and ventral stream signals are integrated to solve this task. We found that a distinct neural network is recruited in WS, namely, a parallel medial dorsal pathway, in response to the performance-matched 3-D SFM task as compared with the control group in the presence of a relatively lower degree of activation in the ventral stream regions. Under such conditions, we could establish the neural substrates of reorganization hypothesis that was suggested by our previous EEG study (Bernardino et al., 2013).

Accordingly, WS participants showed very different lateral versus medial dorsal activation patterns as compared with controls. They showed activation of more medial parieto-occipital areas (cuneus, precuneus, and retrosplenial cortex) when perceiving 3-D SFM stimuli whereas control participants preferentially recruited areas in the cIPS and the LO (near the hMT^+ area). The areas of increased activation in the control group are in close agreement with the dorsolateral neural correlates of SFM perception found in prior studies. In fact, the cIPS area found in our study (as well as in James et al., 2002) is likely to correspond to POIPS (located at the intersection of IPS and parieto-occipital sulcus; Orban et al., 1999), parieto-occipital junction (Klaver et al., 2008; Paradis et al., 2000), or parietal shape area (Murray et al., 2003). Across studies, this area also exhibited stronger responses for coherent motion than incoherent/random motion. In addition, our findings revealed that, in typically developing participants, the cIPS strongly responds to relatively simple motion as well as to high-level visual categorical stimuli. These findings are in accordance with the notion that cIPS is involved in analysis of surface pattern orientation, in orientation discrimination tasks, and in coding 3-D features of objects (Grefkes & Fink, 2005). In fact, Murray and colleagues (2003) found that the area they described as parietal shape area (equivalent to our cIPS) albeit activating for SFM stimuli also responds to 3-D line drawings, which led authors to suggest the involvement of this area in shape perception.

Importantly, our results indicated that WS participants fail to activate the dorsolateral cIPS area in the same way control participants do. Previous fMRI studies also demonstrated hypoactivation in regions in the dorsal stream immediately adjacent to the IPS in visuospatial tasks (Sarpal et al., 2008; Meyer-Lindenberg et al., 2004). Such findings may be explained by previous evidence of morphological abnormalities in the IPS in this disorder (Meyer-Lindenberg, Mervis, & Berman, 2006).

The involvement of LO (near hMT^+ area) in SFM perception was also previously reported in typical developing adults (Murray et al., 2003; Orban et al., 1999). In this study, we found increased activation in the control group as compared with the WS group, suggesting that the latter fails in recruiting this area in the lateral part of the occipito-parietal cortex to process coherent motion stimuli.

Previous studies have also reported that ventral stream regions respond to 3-D SFM stimuli in typically developing adults (Klaver et al., 2008; James et al., 2002; Orban et al., 1999). We found subtle group differences in this visual processing stream, which indicates that the processing along the ventral visual stream in WS may also be slightly atypical. Importantly, differences along the ventral visual stream were restricted to the degree of activation (in response to high-level categorical stimuli) and do not suggest the presence of a functional reorganization within this visual stream as occurred in the dorsal stream. These

observations are consistent with the evidence that ventral visual processing is altered in this clinical population gathered by a study focused on visual processing in the FFA region observed in WS group (O'Hearn et al., 2011; Golarai et al., 2010), which showed similar location but larger activation clusters with performance on ventral stream tasks reaching normal or near-normal levels (Deruelle, Rondan, Mancini, & Livet, 2006; Paul et al., 2002).

Concerning the pattern of brain activation found in the WS group in response to SFM stimuli, we verified the above-mentioned lateral to medial surprising occipito-parietal shift of brain activity patterns. This was especially pronounced in the cuneus, precuneus, and retrosplenial cortex. Interestingly, we observed the involvement of retrosplenial cortex and cuneus in motion processing in the WS group. These results suggest that the shift to the midline in the areas activating for the SFM stimuli in WS may be already driven by the differential pattern of motion processing in this disorder.

These results may be framed into the recent findings of Pitzalis, Bozzacchi, et al. (2013) who demonstrated in EEG and fMRI experiments that motion signals flow in parallel from the occipital pole to the medial and lateral motion areas V6 and MT^+, respectively. The fact that WS participants recruit more medial areas (cuneus—V6 and retrosplenial cortex) to process coherent motion suggest that they predominantly use the medial pathway for motion coherence computations whereas controls favor the lateral pathway (hMT^+). Thus, our results also support the evidence of parallel flow of information in medial and lateral parts of the dorsal visual stream for motion processing as proposed by Pitzalis, Bozzacchi, et al. (2013). Such hypothesis is strengthened by previous case studies from our group that demonstrated damage in dorsal stream areas, V3A and V6, in patients with unilateral parieto-occipital lesions whereas area hMT^+ showed normal responses to motion contrast (Duarte et al., 2013; Castelo-Branco et al., 2006).

Recent evidence showing impaired global pattern discrimination in a patient with IPS damage suggest that the perception of global coherent configurations seems to recruit a dorsal visual route (Lestou, Lam, Humphreys, Kourtzi, & Humphreys, 2013). This is in line with the visual profile described in WS with predominant local visual bias in addition to impaired global coherent perception linked to dorsal stream vulnerability (Bernardino et al., 2012). Accordingly, it was shown that the ability to perceive global coherent shapes in patients with damage to dorsal occipito-parietal cortex is performed through the (more medial) recruitment of precuneus (Himmelbach, Erb, Klockgether, Moskau, & Karnath, 2009). The same pattern of activation was found in our clinical group, which consolidates the view of a medial route in the dorsal stream as an alternative pathway to extract 3-D global configurations when dorsal stream vulnerability is present. This study suggests that, in the presence of dorsal stream dysfunction, the medial pathway is the one preferentially recruited to partly compensate for the resulting impairments. In fact, it may be the existence of this parallel pathway in medial parts of the dorsal stream that facilitates the occurrence of this reorganization in WS.

In summary, this study investigated functional reorganization in WS, a cognitive model of dorsal stream vulnerability. We found a substantial reorganization of the dorsal visual stream, in response to 3-D SFM stimuli. In WS, the pattern of activation medially shifted to the cuneus, precuneus, and retrosplenial cortex, featuring an occipito-parietal shift to the midline as compared with controls (cIPS and LO). In contrast, areas along the ventral visual stream in WS appear to exhibit only subtle differences in the degree of activation, which occurs in the same regions as in the control group. Our findings may be interpreted in the light of recent evidence for parallel motion processing in medial (V6) and lateral (hMT^+) parts of the dorsal stream (Pitzalis, Bozzacchi, et al., 2013). The presence of an alternative medial pathway provides a neural substrate for reorganization, whose functional properties are to be addressed in future studies.

Acknowledgments

This work was supported by grants FP7-HEALTH-2013-INNOVATION-1-602186–BRAINTRAIN and COMPETE, PEst-C/SAU/UI3282/2013.

Reprint requests should be sent to Miguel Castelo-Branco, Visual Neuroscience Laboratory, IBILI-Faculty of Medicine, University of Coimbra, Azinhaga de Santa Comba, 3000-354 Coimbra, Portugal, or via e-mail: mcbranco@ibili.uc.pt.

REFERENCES

Atkinson, J., Braddick, O., Anker, S., Curran, W., Andrew, R., & Wattam-Bell, J. (2003). Neurobiological models of visuospatial cognition in children with Williams syndrome: Measures of dorsal-stream and frontal function. *Developmental Neuropsychology, 23,* 139–172.

Atkinson, J., Braddick, O., Rose, F. E., Searcy, Y. M., Wattam-Bell, J., & Bellugi, U. (2006). Dorsal-stream motion processing deficits persist into adulthood in Williams syndrome. *Neuropsychologia, 44,* 828–833.

Atkinson, J., King, J., Braddick, O., Nokes, L., Anker, S., & Braddick, F. (1997). A specific deficit of dorsal stream function in Williams' syndrome. *NeuroReport, 8,* 1919–1922.

Bernardino, I., Castelhano, J., Farivar, R., Silva, E. D., & Castelo-Branco, M. (2013). Neural correlates of visual integration in Williams syndrome: Gamma oscillation patterns in a model of impaired coherence. *Neuropsychologia, 51,* 1287–1295.

Bernardino, I., Mouga, S., Almeida, J., van Asselen, M., Oliveira, G., & Castelo-Branco, M. (2012). A direct comparison of local-global integration in autism and other developmental disorders: Implications for the central coherence hypothesis. *PLoS One, 7,* 1–11.

Blomberg, S., Rosander, M., & Andersson, G. (2006). Fears, hyperacusis and musicality in Williams syndrome. *Research in Developmental Disabilities, 27,* 668–680.

Boddaert, N., Mochel, F., Meresse, I., Seidenwurm, D., Cachia, A., Brunelle, F., et al. (2006). Parieto-occipital grey matter abnormalities in children with Williams syndrome. *Neuroimage, 30,* 721–725.

Cardin, V., & Smith, A. T. (2009). Sensitivity of human visual and vestibular cortical regions to egomotion-compatible visual stimulation. *Cerebral Cortex, 20,* 1964–1973.

Castelo-Branco, M., Mendes, M., Sebastiao, A. R., Reis, A., Soares, M., & Saraiva, J. (2007). Visual phenotype in Williams-Beuren syndrome challenges magnocellular theories explaining human neurodevelopmental visual cortical disorders. *Journal of Clinical Investigation, 117,* 3720–3729.

Castelo-Branco, M., Mendes, M., Silva, M. F., Januario, C., Machado, E., & Pinto, A. (2006). Specific retinotopically based magnocellular impairment in a patient with medial visual dorsal stream damage. *Neuropsychologia, 44,* 238–253.

Deruelle, C., Rondan, C., Mancini, J., & Livet, M. O. (2006). Do children with Williams syndrome fail to process visual configural information? *Research in Developmental Disabilities, 27,* 243–253.

Duarte, I. C., Cunha, G., Castelhano, J., Sales, F., Reis, A., & Cunha, J. P. (2013). Developmental dissociation of visual dorsal stream parvo and magnocellular representations and the functional impact of negative retinotopic BOLD responses. *Brain and Cognition, 83,* 72–79.

Eckert, M. A., Galaburda, A. M., Karchemskiy, A., Liang, A., Thompson, P., Dutton, R. A., et al. (2006). Anomalous sylvian fissure morphology in Williams syndrome. *Neuroimage, 33,* 39–45.

Epstein, R., Harris, A., Stanley, D., & Kanwisher, N. (1999). The parahippocampal place area: Recognition, navigation, or encoding? *Neuron, 23,* 115–125.

Farivar, R., Blanke, O., & Chaudhuri, A. (2009). Dorsal–ventral integration in the recognition of motion-defined unfamiliar faces. *Journal of Neuroscience, 29,* 5336–5342.

Galletti, C., Fattori, P., Gamberini, M., & Kutz, D. F. (1999). The cortical visual area V6: Brain location and visual topography. *European Journal of Neuroscience, 11,* 3922–3936.

Golarai, G., Hong, S., Haas, B. W., Galaburda, A. M., Mills, D. L., & Bellugi, U. (2010). The fusiform face area is enlarged in Williams syndrome. *Journal of Neuroscience, 30,* 6700–6712.

Graewe, B., De Weerd, P., Farivar, R., & Castelo-Branco, M. (2012). Stimulus dependency of object-evoked responses in human visual cortex: An inverse problem for category specificity. *PLoS One, 7,* e30727.

Graewe, B., Lemos, R., Ferreira, C., Santana, I., Farivar, R., & De Weerd, P. (2012). Impaired processing of 3-D motion-defined faces in mild cognitive impairment and healthy aging: An fMRI study. *Cerebral Cortex, 23,* 2489–2499.

Grefkes, C., & Fink, G. R. (2005). The functional organization of the intraparietal sulcus in humans and monkeys. *Journal of Anatomy, 207,* 3–17.

Grill-Spector, K., Kourtzi, Z., & Kanwisher, N. (2001). The lateral occipital complex and its role in object recognition. *Vision Research, 41,* 1409–1422.

Haxby, J. V., Gobbini, M. I., Furey, M. L., Ishai, A., Schouten, J. L., & Pietrini, P. (2001). Distributed and overlapping representations of faces and objects in ventral temporal cortex. *Science, 293,* 2425–2430.

Himmelbach, M., Erb, M., Klockgether, T., Moskau, S., & Karnath, H. O. (2009). fMRI of global visual perception in simultanagnosia. *Neuropsychologia, 47,* 1173–1177.

James, T. W., Humphrey, G. K., Gati, J. S., Menon, R. S., & Goodale, M. A. (2002). Differential effects of viewpoint on object-driven activation in dorsal and ventral streams. *Neuron, 35,* 793–801.

Kanwisher, N., McDermott, J., & Chun, M. M. (1997). The fusiform face area: A module in human extrastriate cortex specialized for face perception. *Journal of Neuroscience, 17,* 4302–4311.

Klaver, P., Lichtensteiger, J., Bucher, K., Dietrich, T., Loenneker, T., & Martin, E. (2008). Dorsal stream development in motion and structure-from-motion perception. *Neuroimage, 39,* 1815–1823.

Lestou, V., Lam, J. M., Humphreys, K., Kourtzi, Z., & Humphreys, G. W. (2013). A dorsal visual route necessary for global form perception: Evidence from neuropsychological fMRI. *Journal of Cognitive Neuroscience, 26,* 1–14.

Mendes, M., Silva, F., Simoes, L., Jorge, M., Saraiva, J., & Castelo-Branco, M. (2005). Visual magnocellular and structure from motion perceptual deficits in a neurodevelopmental model of dorsal stream function. *Brain Research, Cognitive Brain Research, 25,* 788–798.

Meyer-Lindenberg, A., Kohn, P., Mervis, C. B., Kippenhan, J. S., Olsen, R. K., & Morris, C. A. (2004). Neural basis of genetically determined visuospatial construction deficit in Williams syndrome. *Neuron, 43,* 623–631.

Meyer-Lindenberg, A., Mervis, C. B., & Berman, K. F. (2006). Neural mechanisms in Williams syndrome: A unique window to genetic influences on cognition and behaviour. *Nature Reviews Neuroscience, 7,* 380–393.

Murray, S. O., Olshausen, B. A., & Woods, D. L. (2003). Processing shape, motion and three-dimensional shape-from-motion in the human cortex. *Cerebral Cortex, 13,* 508–516.

O'Hearn, K., Roth, J. K., Courtney, S. M., Luna, B., Street, W., & Terwillinger, R. (2011). Object recognition in Williams syndrome: Uneven ventral stream activation. *Developmental Science, 14,* 549–565.

Oldfield, R. C. (1971). The assessment and analysis of handedness: The Edinburgh inventory. *Neuropsychologia, 9,* 97–113.

Orban, G. A., Sunaert, S., Todd, J. T., Van Hecke, P., & Marchal, G. (1999). Human cortical regions involved in extracting depth from motion. *Neuron, 24,* 929–940.

Paradis, A. L., Cornilleau-Peres, V., Droulez, J., Van De Moortele, P. F., Lobel, E., & Berthoz, A. (2000). Visual perception of motion and 3-D structure from motion: An fMRI study. *Cerebral Cortex, 10,* 772–783.

Paul, B. M., Stiles, J., Passarotti, A., Bavar, N., & Bellugi, U. (2002). Face and place processing in Williams syndrome: Evidence for a dorsal–ventral dissociation. *NeuroReport, 13,* 1115–1119.

Peuskens, H., Claeys, K. G., Todd, J. T., Norman, J. F., Van Hecke, P., & Orban, G. A. (2004). Attention to 3-D shape, 3-D motion, and texture in 3-D structure from motion displays. *Journal of Cognitive Neuroscience, 16,* 665–682.

Pitzalis, S., Bozzacchi, C., Bultrini, A., Fattori, P., Galletti, C., & Di Russo, F. (2013). Parallel motion signals to the medial and lateral motion areas V6 and MT+. *Neuroimage, 67,* 89–100.

Pitzalis, S., Fattori, P., & Galletti, C. (2013). The functional role of the medial motion area V6. *Frontiers in Behavioral Neuroscience, 6,* 91.

Pitzalis, S., Sereno, M. I., Committeri, G., Fattori, P., Galati, G., & Patria, F. (2010). Human v6: The medial motion area. *Cerebral Cortex, 20,* 411–424.

Reiss, J. E., Hoffman, J. E., & Landau, B. (2005). Motion processing specialization in Williams syndrome. *Vision Research, 45,* 3379–3390.

Rutter, M., Bailey, A., & Lord, C. (2003). *Social Communication Questionnaire*. Los Angeles: Wertern Psychological Services.

Sarpal, D., Buchsbaum, B. R., Kohn, P. D., Kippenhan, J. S., Mervis, C. B., & Morris, C. A. (2008). A genetic model for

understanding higher order visual processing: Functional interactions of the ventral visual stream in Williams syndrome. *Cerebral Cortex, 18,* 2402–2409.
Schendan, H. E., & Stern, C. E. (2007). Mental rotation and object categorization share a common network of prefrontal and dorsal and ventral regions of posterior cortex. *Neuroimage, 35,* 1264–1277.
Tootell, R. B., Mendola, J. D., Hadjikhani, N. K., Ledden, P. J., Liu, A. K., & Reppas, J. B. (1997). Functional analysis of V3A and related areas in human visual cortex. *Journal of Neuroscience, 17,* 7060–7078.
Tootell, R. B., Reppas, J. B., Kwong, K. K., Malach, R., Born, R. T., & Brady, T. J. (1995). Functional analysis of human MT and related visual cortical areas using magnetic resonance imaging. *Journal of Neuroscience, 15,* 3215–3230.
Troje, N. F., & Bulthoff, H. H. (1996). Face recognition under varying poses: The role of texture and shape. *Vision Research, 36,* 1761–1771.
Ungerleider, L. G., & Mishkin, M. (1982). Two cortical visual systems. In D. J. Ingle, M. A. Goodale, & R. J. W. Mansfield (Eds.), *Analysis of visual behavior* (pp. 549–586). Cambridge, MA: MIT Press.
Wall, M. B., & Smith, A. T. (2008). The representation of egomotion in the human brain. *Current Biology, 18,* 191–194.
Wallach, H., & O'Connell, D. N. (1953). The kinetic depth effect. *Journal of Experimental Psychology, 45,* 205–217.
Wechsler, D. (2003). *Manual for the Intelligence Scale for Children*. Lisbon: Cegoc-Tea.
Wechsler, D. (2008). *Manual for the Intelligence Scale for Adults*. Lisbon: Cegoc-Tea.